RESEARCH ARTICLE

Cu(I) Coordination Compounds Conjugated to Au Nanorods for Future Applications in Drug Delivery: Insights in Molecular, Electronic and Cu Local Structure in Solid and Liquid Phase

Alberto Lopez[a], Simone Amatori[a], Elena Olivieri[a], Iole Venditti[a], Giovanna Iucci[a], Carlo Meneghini[a], Federica Bertelà[a], Fabio Del Bello[b], Wilma Quaglia[b], Maura Pellei[c], Carlo Santini[c], and Chiara Battocchio*[a]

[a] Dr. A. Lopez, Dr. S. Amatori, Dr. E. Olivieri, Prof. I. Venditti, Prof. G. Iucci, Prof. C. Meneghini, Dr. F. Bertelà, Prof. C. Battocchio
Department of Sciences
Roma Tre University
Via della Vasca Navale 79, 00146, Rome, Italy
E-mail: chiara.battocchio@uniroma3.it

[b] Prof. F. Del Bello, Prof. W. Quaglia
School of Pharmacy, Medicinal Chemistry Unit
University of Camerino
Via Madonna delle Carceri (ChIP), 62032 Camerino, Macerata, Italy

[c] Prof. M. Pellei, Prof. C. Santini
School of Science and Technology, Chemistry Division
University of Camerino
Via Madonna delle Carceri (ChIP), 62032 Camerino, Macerata, Italy

Supporting information for this article is given via a link at the end of the document.

Abstract: In the framework of the design, synthesis and testing of a library of copper complexes and nanostructured assemblies potentially endowed with antitumor and antiviral activity and useful for several applications, from drugs and related delivery systems to the development of biocidal nanomaterials, we present the detailed spectroscopic investigation of the molecular and electronic structure of copper-based coordination compounds and of a new conjugated system obtained by grafting Cu(I) complexes to gold nanorods. More in detail, the electronic and molecular structures of two Cu complexes and one AuNRs/Cu-complex adduct were investigated by X-ray photoelectron spectroscopy (XPS), synchrotron-induced XPS (SR-XPS) and near edge X-ray absorption spectroscopy (NEXAFS) in solid state, and the local structure around copper ion was assessed by X-ray absorption spectroscopy (XAS) both in solid state and water solution for the AuNRs/Cu-complex nanoparticles. The proposed multi-technique approach allowed to properly define the coordination geometry around the copper ion, as well as to ascertain the molecular structures of the coordination compounds, their stability and modifications upon interaction with gold nanoparticles, by comparing solid state and liquid phase data.

Introduction

Lonidamine (LND) is an antineoplastic drug able to sensitize tumors to radio-, chemo- and photodynamic-therapy,[1] by inhibiting mitochondrial respiration and glycolysis.[2] It is able to increase the efficacy of traditional chemotherapeutic agents, including cisplatin and other Pt-based drugs.[3] Moreover, a recent and promising approach concerned the preparation and biological study of gold nanoparticles conjugated with LND and aptamer AS1411 as an effective anticancer strategy.[4]

Copper complexes and copper-based nanodrugs might be promising antitumor agents due to the elevated need for copper by cancer tissues in comparison with normal cells and its role as a limiting factor for multiple aspects of tumor progression.[5,6] In addition, antiviral activity against different infectious DNA or RNA viruses has been reported for copper complexes and, in general, nano-sized Cu(I) compounds have greater antiviral activity than Cu(II) ones.[7,8]

Recently, we have functionalized LND with species able to coordinate metals, to obtain Cu(I) and Cu(II) complexes potentially capable to exert an anticancer activity through synergistic mechanisms of action.[9] The coordination geometry and molecular structure of the synthesized complexes have been assessed by X-ray Absorption Spectroscopy (XAS) and X-ray Photoemission Spectroscopy (XPS). The spectroscopic analysis allowed to investigate in detail the electronic structure of the Cu(I) coordination compounds, as well as the electronic interaction arising between the metal ion and the ligands. In particular, XPS enabled us to specifically probe the ligand-metal interaction and to evaluate the coordination compounds' molecular stability, providing an accurate description of their molecular and electronic structures, in comparison with the pristine ligands. XAS measurements performed at the Cu K-edge allowed to ascertain the coordination geometry at the copper ion site. The assessment of the electronic interaction between the metal ion and the ligands and the investigation of the copper ion oxidation state stability could be of primary importance for a better comprehension of the biological activity.

Here, we report the detailed structural and electronic investigation carried out on two copper(I) coordination compounds,

$[(PTA)_2Cu(L^3)]PF_6$ (**1**) and $[(PPh_3)_2Cu(L^3)]PF_6$ (**2**), aiming at determining their electronic, molecular structure and local arrangement around the copper ion. Among the two investigated complexes, the best performing one in terms of chemical structure stability has been conjugated to gold nanorods (AuNRs) and the obtained nanosystem has also been investigated in terms of electronic, molecular and local structure at both Cu and Au edges. Finally, XAS measurements have been also carried out on aqueous solutions of the AuNRs/Cu-complex $[(PTA)_2Cu(L^3)]PF_6$ (**1**) adduct (namely AuNRs-(**1**)), to probe the system behavior in water, a mandatory step in view of the envisaged applications in the field of drug-delivery.

Materials and Methods

Synthesis

The ligand L^3 and the related complexes **1** and **2** were prepared according to the procedure reported in **Scheme 1**.[9]

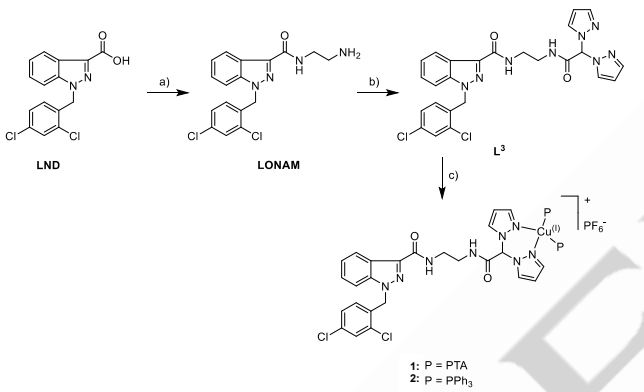

Scheme 1. Synthesis of ligand L^3 and complexes **1** and **2**. Reagents and conditions: a) $H_2NCH_2CH_2NH_2$, CDI, THF, r.t., 18 h; b) $HC(pz)_2COOH$, HOBT, EDCI·HCl, DMF, r.t., 16 h; c) PTA or PPh_3, $Cu(CH_3CN)_4PF_6$, CH_3CN, overnight.

In particular, treatment of LND with ethylenediamine in the presence of carbonyldiimidazole (CDI), at room temperature, led to the intermediate LONAM, which reacted with $HC(pz)_2COOH$ in the presence of 3-(ethyliminomethylideneamino)-*N*,*N*-dimethyl-propane-1-amine hydrochloride (EDCI·HCl) and 2-hydroxybenzotriazole (HOBT), at room temperature, to give ligand L^3. The analytically pure copper(I) complexes $[(PTA)_2Cu(L^3)]PF_6$ (**1**) and $[(PPh_3)_2Cu(L^3)]PF_6$ (**2**) were synthesized by a one-step reaction of the ligand L^3 and $[Cu(CH_3CN)_4]PF_6$ with an excess of 1,3,5-triaza-7-phosphaadamantane (PTA) or triphenylphosphine (PPh_3), respectively, in acetonitrile solution at room temperature (**Scheme 1**). The crude $[(PTA)_2Cu(L^3)]PF_6$ was filtered and subsequently purified in diethyl ether (50 mL) and then in n-hexane (50 mL) to obtain the crystalline white complex **1**. Analogously, the crude $[(PPh_3)_2Cu(L^3)]PF_6$ was filtered and purified in diethyl ether (50 mL) to obtain the white complex **2**.[9]
The AuNRs, prepared by literature procedure,[10] and Cu(I) complex **1**, were mixed in water (Au/**1** = 5/1 w/w) under gentle stirring at room temperature (25 °C). After 4 h the suspension was centrifuged (13,000 rpm, 2 h) to obtain the conjugated system AuNRs-(**1**) as a solid residue, in analogy with past work.[11]

Spectroscopic Methods

X-ray photoelectron spectroscopy (XPS) measurements were carried out using a custom designed spectrometer, described in previous studies[12] and equipped with a non-monochromatized Mg Kα X-ray source (photon energy = 1253.6 eV, pass energy = 25 eV, step = 0.1 eV). For this experiment, photoelectrons emitted by C1s, O1s, N1s, Cl2p, P2p, F1s, Cu2p core levels were detected on solid state samples (powders) of complexes **1** and **2**. All spectra were energy referenced to the C1s signal of aromatic C atoms having a binding energy BE = 284.7 eV.[13] Atomic ratios were calculated from peak intensities using Scofield's cross-section values.[14] Curve-fitting analysis was performed using Gaussian profiles as fitting functions, after subtraction of a polynomial background. For qualitative data, the BE values were referred to NIST database.[15]

Synchrotron Radiation-induced XPS (SR-XPS) experiments at high resolution were performed at the TEMPO beamline at the French national synchrotron radiation facility SOLEIL; TEMPO is a soft-x-ray beamline designed for time dependent studies of electronic and magnetic properties of materials using photoelectron spectroscopy experiments, equipped with two APPLE II helical insertion devices that have periods of 44 mm and 80 mm allowing to cover the whole energy range of the beamline using the first harmonic. The beamline main experimental station is dedicated to UHV photoelectron spectroscopy experiments; it is composed by a main UHV chamber, a preparation chamber and a manipulator section. The main chamber is equipped with a Scienta SES 2002 electron energy analyzer and a LEED system (Specs) placed at the photon beam level. An Omniax manipulator with a travel of 600 mm is placed vertically and it can move from the topmost level in the manipulation section to the bottom level for sample transfer. The resolving power E/ΔE is higher than 10.000 for all energy range; the spot at the sample is 300 µm x 300 µm.[16] SR-XPS data were collected on the sample obtained by conjugating the Cu(I) coordination compound **1** with gold nanorods (AuNRs-(**1**)); measurements were carried out in solid state on AuNRs-(**1**) deposited onto TiO_2/Si(111) wafer surfaces by following a drop-casting procedure from water suspension. Core-level C1s, N1s, Ag3d spectra were acquired using a photon energy of 500 eV; for Cu2p, C1s (calibration) signals a photon energy of 1100 eV was selected; finally, C1s (calibration), Br3d, Cl2p, P2p and Au4f spectra were collected using a photon energy of 360 eV, as to maximize signals cross sections and intensities. All spectra were energy referenced to the C 1s signal of aliphatic C atoms having a binding energy BE 285.0 eV, due to the large amount of cetyl ammonium bromide (CTAB) C-C groups on the AuNRs surface. Curve-fitting analysis was performed using Gaussian profiles as fitting functions, after subtraction of a polynomial background. For qualitative data, the BE values were referred to NIST database.[15]
X-ray Absorption Spectroscopy (XAS) measurements were carried out at the Cu K-edge (8979 eV), at the B18 beamline at Diamond Synchrotron Radiation Facility.[17] Solid samples were prepared by grinding sample powders with boron nitride then pressed to obtain solid pellets suitable for handling. Pellets were mounted in liquid nitrogen (LN) cryostat and measured in transmission geometry. Samples AuNRs-(**1**) (solid state) and

AuNRs-H_2O-(**1**) (aqueous solution) were obtained, one as dried powder of complex **1** after reaction with AuNRs, the other as an aqueous solution of AuNRs-(**1**). In both cases the presence of Cu is in ultra-diluted amount, and the detectability of the Cu signal is a challenge, especially for EXAFS measurements. Samples in solutions were measured in the liquid sample cell, frozen to the LN temperature and XAS data were collected in fluorescence geometry. Incident x-ray intensity I_o was monitored using a gas filled ionization chamber. Transmitted intensity I_t was measured using a second ionization chamber after the sample and the XAS signal calculated as $\alpha_t = \ln(I_o/I_t)$, the total fluorescence yield was measured using a 36 Ge-multidetector, processed with the multichannel electronics to select the Cu-K_α emission $I_{f(i)}$. The $I_{f(i)}$ data were processed by removing glitches and Bragg peaks and averaged, and the XAS signal was calculated as $\alpha_f = \sum_{i=1}^{36} I_{f(i)}/I_o$. A Cu-metal foil was placed after the I_t chamber and its transmitted intensity I_r was measured with a third ionization chamber, the reference XAS signal was calculated as $\alpha_r = \ln(I_t/I_r)$. Several scans were measured to improve the data statistics, checked for energy alignment, and averaged to improve the data statistics; for AuNRs-H_2O-(**1**) 41 scans were acquired and for AuNRs-**(1)**, 141 scans were acquired. To avoid the effects of radiation damage, the samples were shifted slightly with each scan, so that a different spot is illuminated with each scan.[18] In these two last samples the very diluted amount of Cu prevented the possibility to extend the analysis to the extended region (EXAFS) and the data were considered only in the near edge (XANES) region. The XANES region, being dense of structural and electronic details,[19] can be used to extract valuable details about the average absorber valence state and coordination geometry, also by comparison with reference compounds.

All experimental spectra α_{exp}, were treated using the standard procedures for background subtraction and normalization[19] including the linear pre-edge subtraction ($\alpha' = \alpha_{exp} - \alpha_{pre}$), bare atomic background (α_b) subtraction, and normalization. The EXAFS structural signal is expressed as $\chi_{exp}(k) = (\alpha' - \alpha_b)/\alpha_b$ and the XANES normalized spectra as $\mu(E) = \alpha'/\alpha_b$. The edge energy E_o, origin of the photoelectron wavenumber $k = \hbar^{-1}\sqrt{2m_e(E - E_0)}$ (m_e being the electron mass) was defined at the first inflection point (maximum of the first derivative) of the pre-edge subtracted spectra α'.

The quantitative analysis of the EXAFS signals was carried out on the solid state (powder) complexes **1** and **2,** fitting the k^2-weighted theoretical curves $k^2\chi_{theo}$ to the raw experimental data $k^2\chi_{exp}$, in the 3-15 $Å^{-1}$ k range. The analyses applied to the selected ranges consist in a not linear least-square procedure implemented in the program FitEXA. [20] The theoretical curves χ_{theo} were calculated as a sum of partial contributions calculated using the standard EXAFS formula using a gaussian proximation for the structural disorder.[21,22] The theoretical photoelectron scattering amplitude and phase functions were calculated using FEFF8 program[23] using model atomic clusters based on reference compounds structures and DFT modelling.[9]

Near Edge X-ray Absorption Fine Structure (NEXAFS) spectroscopy was carried out at the BEAR beamline (Bending magnet for Emission Absorption and Reflectivity) at the ELETTRA storage ring. BEAR is installed at the left exit of the 8.1 bending magnet exit. The apparatus is based on a bending magnet as a source and beamline optics delivering photons from 5 eV up to about 1600 eV with selectable degree of ellipticity. The UHV end station is equipped with a movable hemispherical electron analyzer and a set of photo-diodes to collect angle-resolved photoemission spectra, optical reflectivity, and fluorescence yield. In these experiments, we used ammeters to measure drain current from the sample. N-K edge spectra were collected at grazing (20°) and magic (54.7°) incidence angle of the linearly polarized photon beam with respect to the sample surface. The raw spectra were normalized to the incident photon flux by dividing the sample spectrum by the spectrum collected on a freshly sputtered gold surface. Spectra were then normalized by subtracting a straight line that fits the part of the spectrum below the edge and assessing to 1 the value at 430.00 eV.

Results and Discussion

Cu(I) coordination compounds structural investigation

*Molecular and electronic structure of Cu(I) coordination compounds **1** and **2**: X-ray Photoelectron Spectroscopy (XPS) and Near Edge X-ray Absorption Fine Structure (NEXAFS) studies.*

The electronic and molecular structure of coordination compounds **1** and **2** were probed by X-ray Photoelectron Spectroscopy (XPS). XPS spectra were collected at C1s, N1s, O1s, Cl2p, P2p, F1s and Cu2p core levels; the detailed data analysis results (Binding Energy (BE), Full Width Half Maximum (FWHM), and assignments), leading information about the molecular structures of the coordination compounds and the stability of the ligands molecular structure upon coordination to copper, are collected in the Supporting Information (Table S1). In the following, the most interesting signals will be described and compared for the two analysed samples.

The C1s signal can be always resolved by curve fitting analysis into several components corresponding to the different C atoms in the proposed molecular structure. The two coordination compounds have similar molecular structure, differing only for phosphine ligands (PPh_3 or PTA). This allows for a straightforward comparison between the C1s, N1s, O1s and P2p data, that are the most indicative for the correspondence between the observed and proposed molecular structures.

C1s spectra (Figure 1) are composite and by applying a peak fitting procedure it is possible to individuate at least four components, assigned as in the following: aromatic and aliphatic C-C carbons (BE= 284.7 eV), superimposed to C-P signals when present (component C1); C-N carbons of the pyrazole-like rings (BE= 286.1 eV, namely C2), C-Cl[24] (BE = 287.5 eV, component C3), NCOR (BE = 288.7 eV, C4).[15]

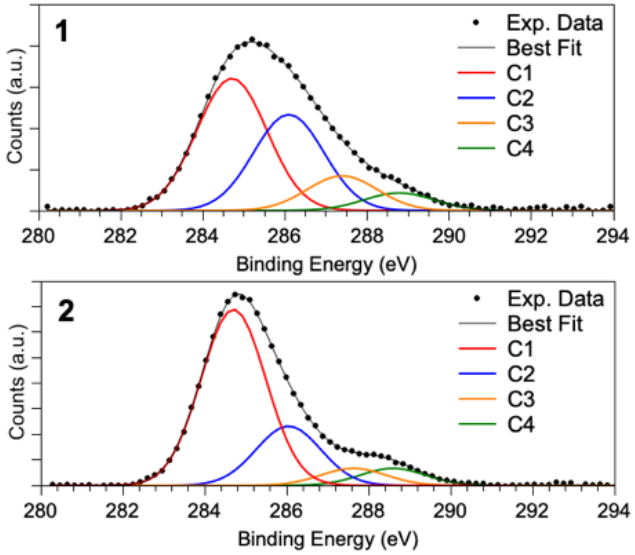

Figure 1. C1s XPS spectra collected on the Cu(I) coordination compounds **1** (top) and **2** (bottom).

The details of the C1s data analysis are summarized in Table 1; it is noteworthy that the experimental atomic ratios calculated for the C1, C2, C3 and C4 components are in good agreement with the theoretical ones**,** based on the hypothesised molecular structure, for **1**, confirming the molecular stability of the ligands upon anchoring the Cu metal ion in this coordination compound. The lower amount of C1 with respect to C4, compared with the theoretical atomic ratios, observed in **2** is probably due to a higher contribution of COOH groups arising by impurities on the sample holder surface (that is usually cleaned with CH_3COOH). This also explains the lower amount of C2 with respect to the same C4.

Table 1. XPS data (BE, FWHM, experimental and theoretical atomic ratios and proposed assignments) for C1s core levels.

Sample	BE (eV)	FWHM (eV)	atomic ratios *Ci/C4 (exp.)	atomic ratios *Ci/C4 (theor.)	Assignment
	284.7	2.0	7.5	8.5	C-C + C-P (C1)
1	286.1	2.0	5.5	4	C-N (C2)
	287.4	2.0	2.0	2	C-Cl (C3)
	288.8	2.0	1.0	1	NCOR (C4)
	284.7	1.9	10.5	23.5	C-C + C-P (C1)
2	286.1	1.9	3.5	5	C-N (C2)
	287.6	1.9	1	1	C-Cl (C3)
	288.6	1.9	1	1	NCOR (C4)

*Ci = C1, C2, C3, C4

Cl2p spectra (see Figure S1a in SI) fully confirm the assignments for C3 component, having a $Cl2p_{3/2}$ signal BE centred around 200.5 eV, as expected for Cl-C in chlorobenzene.[24] The coordination compounds stability and molecular structure consistency with the hypothesised ones is further confirmed by N1s spectra, showing a component for the N atoms coordinating Cu at about 400 eV BE, as expected for the symmetrized pyrrole N in coordination compounds,[9,25] and a second component at higher BE (401.5 eV) arising by imine-like nitrogens (Figure S1b). P2p and F1s signals (Figure S1c and d) also support the proposed chemical structures. A $P2p_{3/2}$ component at 131 - 132 eV BE is always observed and attributed to P atoms of either PPh_3 (**2**) or PTA (**1**); the stability and reproducibility of this component confirms that no oxidation of phosphines, that would suggest a major molecular structure degradation, takes place. A second P2p signal is observed at higher BE ($P2p_{3/2}$ BE = 136 eV) as expected for PF_6^- ions; coherently, F1s signal is always found around 686 eV BE.[15] In addition, the atomic ratio between fluorine atoms and P ascribed to PF_6^- is about 6/1 for **1**, in excellent agreement with the counter-ion stoichiometry (Table S1). Finally, Cu2p spectrum of complex **1** (representative for the Cu2p spectra of both coordination compounds) is reported in Figure 2. As expected, the most intense component in copper spectrum is indicative for Cu(I) ions bonded to phosphines in coordination compounds;[9] however, a signal of small intensity is also observed at higher BE values, and attributed to about 10% of Cu(II), probably due to a low degree of sample degradation. The larger amount of Cu(II) revealed in **2** could also explain the discrepancies observed for the experimental / theoretical atomic ratios in this coordination compound (Table 1 and Table S1).

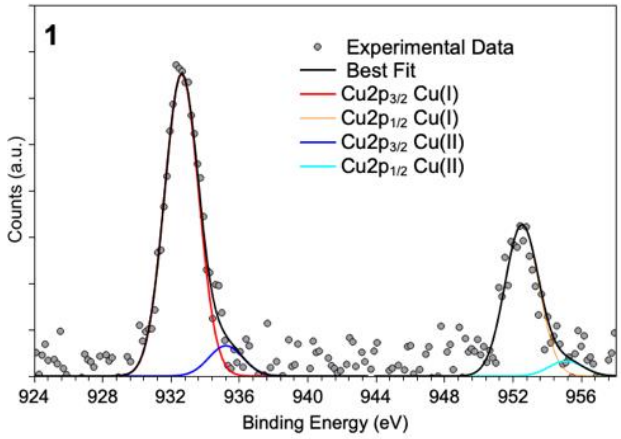

Figure 2. Cu2p spectrum of complex **1**.

Near Edge X-ray Absorption Fine Structure (NEXAFS) spectroscopy measurements were carried out at the N K-edge for complexes **1** and **2**. Spectra were recorded at grazing (20°) and magic (54.7°) incidence of the impinging polarized radiation, but no angle dependent effects were evidenced, apart from a better signal to noise ratio in the more intense grazing incidence spectra. The spectra of the two samples are very similar; the N K edge spectrum of complex **1** recorded at grazing incidence is shown in Figure 3; peak position and assignment are displayed in Table 2.

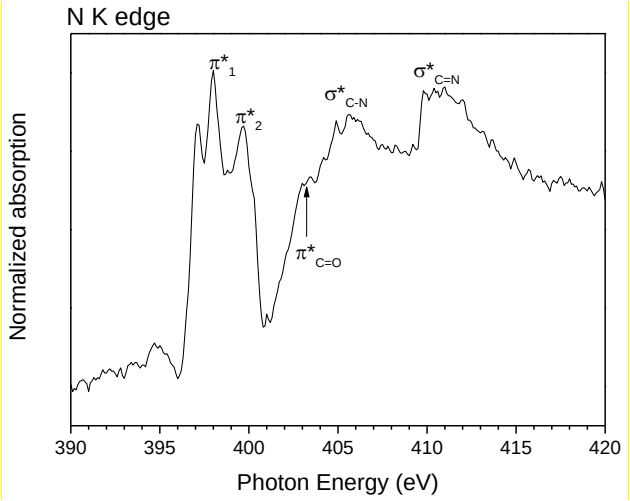

Figure 3. N K edge NEXAFS spectrum of complex **1** recorded at grazing incidence of the impinging polarized radiation.

Table 2. Peak position and relative assignment for the N K edge NEXAFS spectrum of complex **1**.

Peak position (eV)	assignment
397.1	
398	π^*_1
399.6	π^*_2
405.5	σ^*_{C-N}
411	$\sigma^*_{C=N}$

The spectrum shows the typical features related to the 1s→π* resonances of the C=N bonds of the pyrazole rings, labelled π^*_1 and π^*_2 in Figure 3 and Table 2, that are related to transitions arising from the two non-equivalent nitrogen atoms of pyrazoles. The π* resonance related to the amide C=O bonds probably appears as a shoulder on right hand side of the σ* resonances related to C-N and C=N bonds, above the edge.[9]

Local structure around Cu ions: XAS investigation in solid state

The Cu K-edge XAS spectra of complexes **1** and **2** were analysed in both XANES and EXAFS regions, which provide complementary information on the local ordering around the average absorber. The XANES features provide information on the average valence state of the absorber, the density of empty states near the Fermi level, and the symmetry of the coordination environment,[19] while the analysis of the EXAFS data provides further details on the average atomic coordination around the absorber in terms of the average distance, number, and mean squared relative displacement (MSRD) of the neighbouring shells.[21]

The normalized Cu-K edge XANES spectra measured on complexes **1** and **2** are shown in Figure 4 along with the XANES spectra measured on Cu-metal foil, Cu_2O and CuO for the sake of comparison. The quite broad features in the post edge region accounts for the quite disordered nature of the Cu local structure respect to the ordered crystallographic nature of the reference compounds. The edge position of Cu in complexes **1** and **2** (Figure 4) is consistent with the Cu(I) valence state in both materials. The evident peak A at the Cu K-edge spectra of complexes **1** and **2** around 8985 eV, is commonly attributed to the photoelectron transitions from the 1s Cu state to its 4s and 4p ones.[26] The intensity and shape of the A peak directly reveal information about the Cu coordination geometry.[26] linear 2-coordinated Cu has the highest A intensity (close to 1), the A peak intensity around 0.5 is consistent with almost regular tetrahedral coordinated Cu. Tetrahedral coordination is common for Cu(I) in similar complexes with bipirazolyl ligands (see as examples[27,28,29]) and comes in agreement with the DFT models calculated for complexes **1** and **2**, and with the results of the EXAFS analysis. The weak differences can be ascribed to the structural differences and steric constraints of PTA ligands (complex **1**) or PPh_3 (complex **2**) ligands. In the post-edge region (8990-9030 eV) the XANES spectra of the complexes **1** and **2** depict evident differences, due to the different geometries of the atoms of the phosphane ligand and the counterion PF_6^- [9,31] in those two complexes, even if the Cu bonding geometry remains similar.

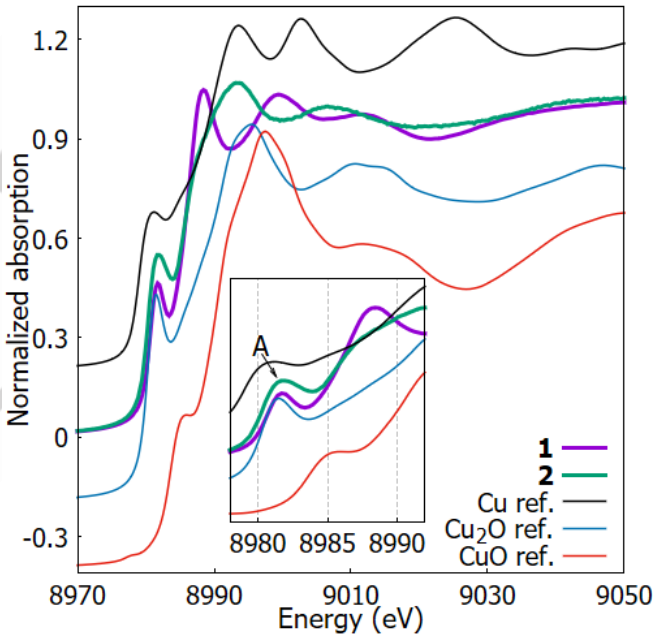

Figure 4. The main image shows the normalized Cu K edge XAFS spectra measured in complexes **1** (purple line) and **2** (green line), along with the spectra of reference compounds: Cu foil (black line), $Cu_2(I)O$ (blue line) and a Cu(II)O (red line), vertically shifted for the sake of clarity. The inset reports a magnification on the edge region of the spectra.

The XAFS signal in the post edge region, some tens eV above the edge (Figure 4), is determined by the full multiple scattering (FMS) signals originating from the ligands and next neighbor shells around the absorber.[32] The higher frequency of fine structure oscillations observed in complex **2** (Figure 4) suggests relevant structural contributions originating from more distant neighbor shells from the PPh_3 groups. Such a difference decreases as one moves away from the edge, in the EXAFS region where the structural signal is dominated by single scattering events from the nearest neighbor shells, while the next-neighbor shell signals are attenuated by the structural disorder [32].

This is evident looking at the $k^2\chi$ EXAFS spectra (Figure 5a): the signals of both samples become quite similar above $k \simeq 3\ \text{Å}^{-1}$. However, looking at the Fourier transforms (Figure 5b) it is still evident a major contribution from next neighbor shells till around 3.5 Å in the data of complex **2**. The quantitative analysis can provide further details.

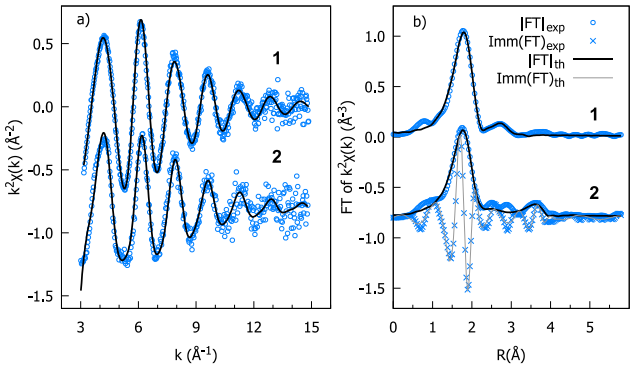

Figure 5. a) experimental data (blue circles) and best fit (black lines) of the k^2-weighted EXAFS spectra for complexes **1** and **2**, vertically shifted for clarity; b) moduli of the Fourier transform (|FT|) of k^2-weighted experimental data ($|FT|_{exp}$, blue circles) and best fit curves ($|FT|_{th}$, black lines) for complexes **1** and **2**, vertically shifted for clarity. For complex **2** also the imaginary part of the FT of the experimental data ($Imm(FT)_{exp}$, blue crosses) and best fit curve ($Imm(FT)_{th}$, grey line) are shown.

The quantitative analysis of Cu K-edge EXAFS spectra has been carried out refining the local atomic around Cu initially based on DFT models of the in the two complexes shown in Figure 1. The relevant contributions were individuated selecting and grouping together structural signals with similar geometry/composition as described in reference[33]. The $k^2\chi(k)$ experimental data and best fit for the complexes **1** and **2** are shown in Figure 5a, along with their Fourier transforms (Figure 5b) providing a more intuitive description of the local structure around Cu in the two samples, the main peak around 2 Å in the |FT| (uncorrected for the phase shift), similar for both the complexes, being ascribed to Cu nearest neighbor shells. Table 3 resumes the best fit parameters for the different contributions (shells) used in the analysis. Details about the signals associated to each shell, theoretical distances and multiplicity refer to Figure S3 and Table S2 in the Supporting Information. To reduce the correlations among the parameters we fixed the multiplicity of the different contributions (shells) to the theoretical values, the same $S_0^2 = 0.9$ (representing the passive electron reduction factor) was applied to all the paths and data sets. The energy scale shift (ΔE_0) was left to change, obtaining 6 eV and 4 eV for complex **1** and complex **2**, respectively.

The main contributions to the EXAS signal are represented by two shells representing the directly bonded neighbors being 2 Cu-N around 2.07 Å and 2 Cu-P around 2.22 Å (Table 3). These shells are very similar in both complexes with slightly broader distribution (σ^2) in complex **2** respect to **1**. The first two shells confirm that the Cu(I) ions are four coordinated to 2N and 2P neighbors in both complexes. The structural signals from next neighbor shells are week, as evident in the Fourier transforms (Figure 5b) but extending the EXAFS analysis provides further details about the Cu(I) coordination chemistry. The third and fourth contributions (S3 and S4 in Table 3) can be ascribed mainly to the single (SS) and selected multiple (MS) scattering contribution of the second shell ($C_{1,2}$ and N_2 atoms in Figure S3) of the chelating ligand L^3, which is common to the two complexes, again the mean square relative displacement (σ^2) is larger for complex **2** pointing out a broader distribution of the neighbors. The S3 shell is slightly closer in complex **2** respect to complex **1** and the opposite is for the S4 contribution, mainly originating from Cu-N_1-C_2(N_2) multiple scattering paths. It is possible that in complex **2** the S4 signal is affected by the Cu-C_{P1} SS signals which are expected around 3.5 Å (see SI and Figure S3). The S5 and S6 contributions are relevant only for complex **2** and allow to account for the evident peak around 3.5 Å (uncorrected for the phase shift) in the FT (Figure 5b). It is difficult to reliably associate a specific coordination shell in this region due to the interference of many overlapping signals, we reproduce this contribution with 4 SS (Cu-C) and 8 MS (Cu-P-C) shells (corresponding to the shells 5 and 6 in Table 3) sharing the same path length (about 4 Å) and σ^2 (about 0.5×10^{-2}Å^2) on the understanding that this is a crude approximation of the actual structure, useful only to emphasize a difference between the coordination of Cu in the two complexes originating from the PPh_3 ligands. The fitted values are in reasonable accordance with the DFT models, considering that the grouping of more paths under the same shell leads to consider all lengths involved in the shell as equal to the average.[21]

Table 3. Structural parameters resulting from the best fit of Cu K edge EXAFS spectra on complexes **1** and **2**. The structural parameters (N: multiplicity, R: average distance, σ^2: mean square relative displacement) are shown for each contribution (shell), the uncertainties on the last digit of the refined parameters are reported in parentheses. The ligand shells (Cu-N_1 Cu-P) and the S3 and S4 contributions are similar for both the samples, the S5 and S6 contributions are specific of complex **2**.

	Complex **1**			Complex **2**		
Shell	N	R (Å)	σ^2 x10^2 (Å^2)	N	R (Å)	σ^2 x10^2 (Å^2)
Cu-N_1	2	2.07(1)	2.0(5)	2	2.06(1)	5.3(9)
Cu-P	2	2.23(2)	0.53 (5)	2	2.22 (2)	0.62(5)
S3 (SS)	5	2.98(2)	1.6(2)	5	2.88(3)	3.4(4)
S4 (MS)	8	3.21(3)	0.78(4)	8	3.39(3)	1.4(2)
S5 (SS)	-	-	-	4	4.03(5)	0.5(3)
S6 (MS)	-	-	-	8	4.03*	0.5*

AuNRs-(1) structural investigation

*Molecular and electronic structure of Cu(I) coordination compound **1** conjugated with AuNRs in solid state: SR-XPS studies.*

SR-XPS measurements were carried out on the nanoparticles AuNRs-(**1**) obtained by conjugating the Cu(I) complex **1**, selected as the most structurally stable among the two by the combined XPS, NEXAFS and XAS structural characterization, with a gold nanorod, as described in the experimental section. SR-XPS data were collected on the solid-state sample deposited onto a TiO_2/Si(111) wafer surface as described in the experimental section; C1s, N1s, P2p, Cl2p, Au4f, Ag3d, Cu2p and Br3d core-level spectra were measured and analysed to obtain information about the coordination compound molecular and electronic structure stability upon interaction with the gold nanorod surface. It is noteworthy that gold nanorods are stabilized by a thick layer of the organic ligand CTAB, as described in previous works,[10,34] then the CTAB core level signals contributions must be also considered when analysing the complex nanosystem SR-XPS spectra.[10] The complete collection of Binding Energy (BE), full width half maxima (FWHM), atomic percentage values and proposed assignments is reported in Table S1 in the Supporting Information; here only the most significative signals related to complex **1** and AuNRs molecular and electronic structure behaviour upon conjugation will be discussed in detail. First, C1s, N1s and Br3d core level signals appear fully consistent with the expected spectra for AuNRs stabilized by CTAB ligand, considering a small contribution arising by the coordination compound **1**. More in detail, as shown in Figure 6a, C1s spectrum of AuNRs-(**1**) is composite and very similar to the pristine coordination compound spectrum reported in Figure 1, with an increased intensity of components C1 (C-C) and C2 (C-N) clearly due to the presence of CTAB aliphatic chains and terminal amine groups. N1s spectrum (Figure 6b) is also structured but, differently from pristine complex **1**, now three peaks can be individuated; by comparison with the SR-XPS data collected on AuNRs,[10] and considering the presence of C-N and C=N contributions arising by **1**, the three spectral contributions can be assigned as follows: N1 (BE = 398.3 eV) N-C amine-like arising by CTAB molecules; N2 (BE = 400.1 eV) N-C amine-like of complex **1**, in excellent agreement with N1s spectra collected on pristine complexes **1** and **2** (see Table S1); N3 (BE = 401.7 eV) superposition of N1s signals arising by N=C imine-like groups of **1** (coherently with pristine compounds data, Table S1) and positively charged nitrogen atoms of the CTA^+ / Br^- / Ag^+ complex formed by CTAB on the AuNRs surface, as previously extensively discussed.[10] Br3d signal (Figure 6c) is due to CTAB only, with the two expected components Br1 ($Br3d_{5/2}$ BE = 68.5 eV) ascribed to bromine atoms of the CTAB external layer, and Br2 ($Br3d_{5/2}$ BE = 69.6 eV) arising by bromine ions at the AuNRs surface in the CTA^+ / Br^- / Ag^+ complex.[10] Au4f spectrum (Figure 6d) confirms the presence of AuNRs, and is coherent with the expected metallic gold; it is noteworthy that Ag3d signal was too noisy to be acquired, probably due to the thick overlayer of CTAB and complex **1** molecules covering the AuNRs surface, that is expected to contain a very low amount of silver atoms and ions, since silver is only introduced in a very low amount as $AgNO_3$ in the AuNRs synthesis to drive the anisotropic growth.[10,34] Finally, $Cu2p_{3/2}$ spectrum acquired at high resolution thanks to the SR allows to unambiguously assess the presence of **1** on the AuNRs surface; as shown in Figure 6e Cu2p signal is composite, showing a first contribution due to Cu(I) (main signal, $Cu2p_{3/2}$ BE = 932.3 eV) and a second peak attributed to Cu(II) ($Cu2p_{3/2}$ BE = 934.3 eV), as already observed in pristine **1** (Figure 2) but of higher intensity. The increased intensity of the Cu(II)-related signal is probably due to a partial oxidation of Cu(I) ions to Cu(II), an expected ageing behaviour due to the high reactivity and low stability of Cu(I) ions.[35] The overall AuNRs-Cu(I) complex stability is suggested by P2p and Cl2p spectra (reported in the Supporting Information as Figure S2), that appear unmodified with respect to the pristine coordination compound, showing both a single spin-orbit pair with the main $2p_{3/2}$ component centred at $P2p_{3/2}$ = 132.6 eV and $Cl2p_{3/2}$ = 200.3 eV, respectively (see Table S1).

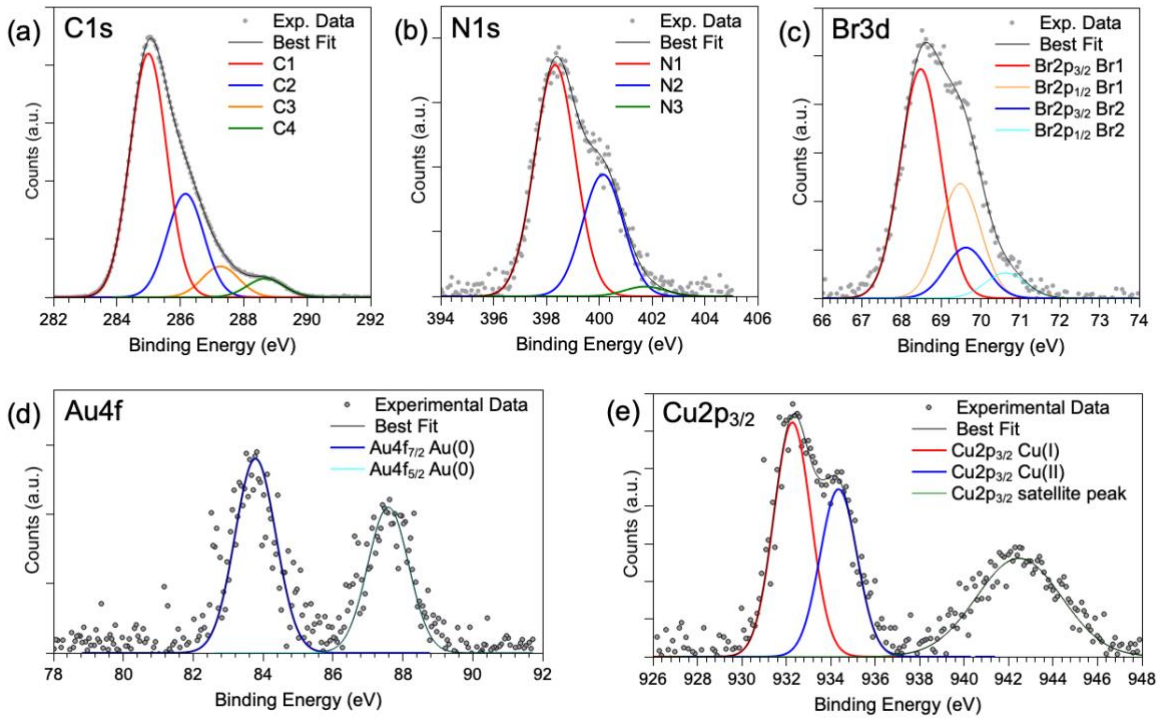

Figure 6. SR-XPS spectra collected on AuNRs-Cu(**1**) in solid state at (a) C1s, (b) N1s, (c) Br3d, (d) Au4f and (e) Cu2p core levels.

XAS in dry AuNRs-(8) and water solution

Being able to look at the XAFS data from Cu in dry AuNRs-(**1**) and water solution AuNRs-H_2O-(**1**) gave us a unique opportunity to get information about the behaviour of Cu site when the complex reacts with AuNRs and with water. Despite a state-of-the-art instrument for XAFS measurements in fluorescence geometry for diluted samples (high flux, high beam stability and reproducibility, 36 element fluorescence detector) and the long time/high number of spectra averaged, the high dilution of Cu in AuNRs-(**1**) and AuNRs-H_2O-(**1**) forced us to restrict the XAFS analysis to the XANES region of the spectra. However, the fine structure features in the XANES region are highly sensitive to the average valence state and coordination geometry of the absorber, making the XANES signal especially suited to individuate structural and/or electronic differences between samples.[19]

The normalized Cu XANES measured on AuNRs-(**1**) and AuNRs-H_2O-(**1**) samples are presented in Figure 7 along with the XANES spectra of reference compounds (Cu_2O, CuO and pure complex **1**) for the sake of comparison. The XANES features measured for the AuNRs-(**1**) and AuNRs-H_2O-(**1**) samples appear very broad and smooth compared to those measured for the dry complex **1**, signaling a much more disordered structure.

The softening of the pre-peak and the broadening of the spectral features in the XANES spectra of Cu in samples AuNRs-(**1**) and AuNRs-H_2O-(**1**) with respect to the spectrum of the dry complex **1** could be attributed to a combination of two effects: the overlap of Cu(I) and Cu(II) absorption signals, ~~sites~~ and the structural distortion of Cu(I) site induced by interaction with AuNR and water.[31,36] The oxidation of Cu(I) to Cu(II) is not surprising from a chemical point of view, due to the in-water deposition of the copper complexes on the AuNRs, and it comes in good agreement with XPS results, showing a large fraction of Cu(II) in AuNRs-(**1**). The finding of Cu(II) in AuNRs-(**1**) EXAFS data not only agrees with the XPS data, but also shows that the presence of Cu(II) is widely distributed throughout the sample volume and not simply confined to the surface layers, as might be expected by the XPS data, which are mainly sensitive to the sample surface due to the short photoelectron mean free path.

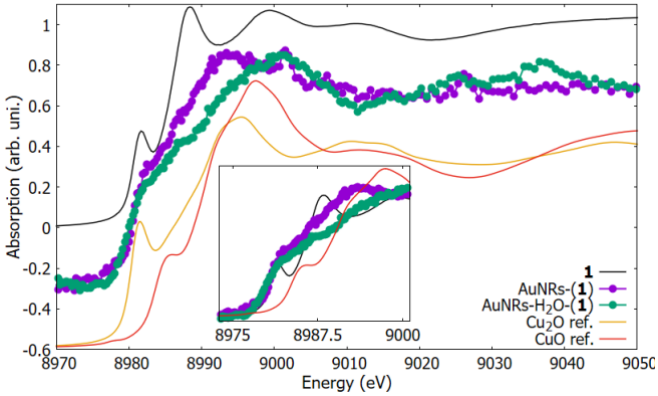

Figure 7. Cu K-edge XANES spectra measured AuNRs-(**1**) and AuNRs-H_2O-(**1**) samples compared with the data of reference compounds and dry complex **1**. In the inset the edge region is highlighted evidencing the difference between the data measured on the dry **1** and on AuNRs-(**1**) (dry and solution) samples.

In order to prove the effect of disorder in the XANES we used FEFF8[23] to calculate ab initio the Cu(I) XANES spectra using the DFT atomic cluster model for the complex **1**. We included the two PTA and the two bi-pyrazolyl ligands till 5.5 Å from the Cu central absorber. The atomic potentials were calculated self-consistently using the Hedin-Lundqvist model within the muffin-tin approximation[23]. The XANES curves and the projected densities of Cu s- and p-states (referred to as s-DOS and p-DOS, respectively) were calculated using the full multiple scattering (FMS) method. To model the complex **1** experimental spectrum the FMS radius was 5.5 Å. The XANES calculated from the DFT atomic model successfully reproduces the key features of the experimental spectrum, validating the model. Notably, the calculated s-DOS aligns well with the observed pre-edge peak (Figure 8), consistently with the established literature. Similarly, the p-DOS peak corresponds to the rising of the Cu edge spectrum.

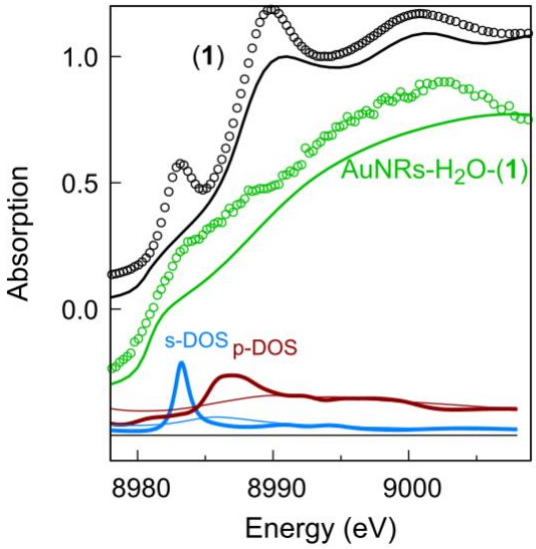

Figure 8. The experimental XANES data (circles) and model curves (full lines) of complex **1** (black) and AuNRs-H_2O-(**1**) samples are shown, vertically shifted for clarity. Bottom curves represent the calculated Cu s- and p-density of states (DOS) for the complex **1** model (tick line) and for the AuNRs-H_2O-(**1**) model (thin lines).

To simulate the impact of structural disorder on XANES spectra for AuNRs-(**1**) and AuNRs-H_2O-(**1**), the disorder has been included using the DEBYE option of FEFF8 program, a standard method for incorporating thermal disorder, and reducing the FMS radius to 4 Å, meaning that the structural disorder weakens the contributions from atoms further away from the absorber. The XANES calculated for the disordered structure becomes progressively broader (the intermediate behaviour of AuNRs-(**1**) model is not shown), and the structural features shift toward higher energy (Figure 4) well matching the experimental trend. A further effect observed in AuNRs-(**1**) and AuNRs-H_2O-(**1**) XANES spectra is the smoothing of the pre-edge peak. Also in this case this effect can be likely ascribed to the flattening of the s- and p-DOS in AuNRs-H_2O-(**1**) model (Figure 4).

The modification of Cu coordination geometry implies a strong interaction of the Cu site of the complex **1** with the AuNRs and/or water molecules. Without more information it is difficult to construct a more accurate and at the same time reliable model of the local Cu structure in the two AuNRs-(**1**) and AuNRs-H_2O-(**1**) samples however, moving from the AuNRs-(**1**) sample (dry) to AuNRs-H_2O-(**1**) (solution) it is evident the high energy shift of the main post-edge oscillations that should be related to a progressive larger disorder in the neighbor shells around the Cu sites. This comes in line with the lipophilic nature of the ligand L^3, which should reduce its contact surface with water, and so squeezing the shape of the complex molecules around the Cu center.

Conclusion

The investigation of the molecular, electronic structure and local geometry of the two copper(I) coordination compounds $[(PTA)_2Cu(L^3)]PF_6$ (**1**) and $[(PPh_3)_2Cu(L^3)]PF_6$ (**2**) reported in this work allowed to unambiguously assess their chemical structure and stability. Following such appraisal, the same experimental approach was applied to the investigation of the nanosystem obtained by conjugating complex **1** to gold nanorods (AuNRs-(**1**)). Since the conjugation procedure is a key step in view of the overseen application of AuNRs-(**1**) as drug-delivery systems for nanomedicine, the comparison between the solid-state structure of AuNRs-(**1**) with the same nanosystem dispersed in water is very interesting. Thanks to the possibility to perform XAS experiments on extremely diluted liquid samples, as required to avoid aggregation of AuNRs-(**1**) particles, the coordination geometry around the copper ion after interaction with the gold nanoparticle was also investigated in liquid phase. The comparison between solid and liquid-phase data suggested a rearrangement of the hydrophilic moiety of Cu(I) complex in presence of water, resulting in a squeezing of the dimensions of the L^3 ligands around the copper center.

Supporting Information

Table S1. XPS data analysis results (BE, FWHM, experimental and calculated atomic ratio values and proposed assignments); Table S2. Shells involved in the EXAFS data analysis of complexes **1** and **2**; the xyz atomic clusters around Cu used for XANES model of complex **1** are listed below the Table. Figure S1. XPS spectra collected at (a) Cl2p, (b) N1s, (c) P2p and (d) F1s core levels for **1**; Figure S2. SR-XPS spectra collected at (a) P2p and (b) Cl2p core levels for AuNRs-(**1**); Figure S3. 3D visual representations of the models used for the EXAFS analysis of complexes **1** and **2**.

The authors have cited additional references within the Supporting Information.[37]

Acknowledgements

This project has received funding from the European Union's Horizon 2020 research and innovation programme under grant agreement No 101007417, having benefited from the access provided by SOLEIL Synchrotron Radiation Facility in Paris – beamline TEMPO - within the framework of the NFFA-Europe Pilot Transnational Access Activity, PID: 383.

Authors from Roma Tre also gratefully acknowledge the following Synchrotron Radiation Facilities: for NEXAFS, ELETTRA (BEAR beamline, proposal #20230160, partially financed); for XAS experiments, Diamond (B18 beamline).

This work was also supported by Unione Europea – NextGenerationEU (MUR-Fondo Promozione e Sviluppo - D.M. 737/2021, INVIRCuM, University of Camerino, FAR 2022 PNR).

The Grant of Excellence Departments 2023–2027, MIUR (ARTICOLO 1, COMMI 314–337 LEGGE 232/2016), and ECS 0000024 Rome Technopole (CUP B83C22002820006, PNRR Missione 4 Componente 2 Investimento 1.5, finanziato dall'Unione europea – NextGenerationEU) are gratefully acknowledged by authors of Roma Tre University.

Keywords: Copper coordination compounds • nanorods • X-ray photoelectron spectroscopy • X-ray absorption spectroscopy • solid and liquid states

[1] K. Nath, L.L. Guo, B. Nancolas, D.S. Nelson, A.A. Shestov, S.C. Lee, J. Roman, R. Zhou, D.B. Leeper, A.P. Halestrap, I.A. Blair, J.D. Glickson, *Biochim. Biophys. Acta, Rev. Cancer* **2016**, *1866 (2)*, 151.

[2] L.L. Guo, A.A. Shestov, A.J. Worth, K. Nath, D.S. Nelson, D.B. Leeper, J.D. Glickson, I.A. Blair, *J. Biol. Chem.* **2016,** *291 (1)*, 42.

[3] R. Angioli, M. Janicek, B. Sevin, R. Estape, H. Averette, O. Koechli, M. Untch, M. Penalver, *Int. J. Oncol.* **1997,** *11(4)*, 777.

[4] H.B. Ruttala, T. Ramasamy, B.K. Poudel, R.R.T. Ruttala, S.G. Jin, H.G. Choi, S.K. Ku, C.S. Yong, J.O. Kim, *Acta Biomater.* **2020,** *101*, 531.

[5] V. Gandin, C. Ceresa, G. Esposito, S. Indraccolo, M. Porchia, F. Tisato, C. Santini, M. Pellei, C. Marzano, *Sci. Rep.* **2017,** *7(1)*, 13936.

[6] C. Santini, M. Pellei, V. Gandin, M. Porchia, F. Tisato, C. Marzano, *Chem. Rev.* **2014**, *114(1)*, 815.

[7] C.N. Banti, N. Kourkoumelis, A.G. Hatzidimitriou, I. Antoniadou, A. Dimou, M. Rallis, A. Hoffmann, M. Schmidtke, K. McGuire, D. Busath, A. Kolocouris, S.K. Hadjikakou, *Polyhedron* **2020**, *185*, 114590.

[8] N. Wang, A.R. Ferhan, B.K. Yoon, J.A. Jackman, N.J. Cho, T. Majima, *Chem. Soc. Rev.* **2021**, *50(17)*, 9741.

[9] F. Del Bello, M. Pellei, L. Bagnarelli, C. Santini, G. Giorgioni, A. Piergentili, W. Quaglia, C. Battocchio, G. Iucci, I. Schiesaro, C. Meneghini, I. Venditti, N. Ramanan, M. De Franco, P. Sgarbossa, C. Marzano, V. Gandin, *Inorg. Chem*. **2022**, *61*, 4919.

[10] S. Amatori, A. Lopez, C. Meneghini, A. Calcabrini, M. Colone, A. Stringaro, S. Migani, I. Khalakhan, G. Iucci, I. Venditti, C. Battocchio, *Nanoscale Adv.,* **2023**, *5*, 3924.

[11] I. Fratoddi, I. Venditti, C. Battocchio, L. Carlini, M. Porchia, F. Tisato, F. Bondino, E. Magnano, M. Pellei, C. Santini, *Nanomaterials*, **2019**, *9*, 772.

[12] V. Secchi, S. Franchi, M. Dettin, A. Zamuner, K. Beranová, A. Vladescu, C. Battocchio, V. Graziani, L. Tortora, G. Iucci, *Nanomaterials* **2020**, *10(6)*, 1151.

[13] J. F. Moulder, W. F. Stickle, P. E. Sobol, K. D. Bomben, Handbook of X-Ray Photoelectron Spectroscopy, Eden Prairie, 1996.

[14] P. Swift, D. Shuttleworth, M.P. Seah in *Practical Surface Analysis by Auger and X-ray Photoelectron Spectroscopy*, (Eds.: D. Briggs and M. P. Seah), J. Wiley & Sons, Chichester, **1983**, chapter 5 and appendix 3

[15] NIST X-ray Photoelectron Spectroscopy Database, Version 4.1 (National Institute of Standards and Technology, Gaithersburg, 2012); http://srdata.nist.gov/xps/. (accessed: January 16th 2024).

[16] F. Polack, M.G. Silly, C. Chauvet, B. Lagarde, N. Bergeard, M. Izquierdo, O. Chubar, D. Krizmancic, M. Ribbens, J.P. Duval, C. Basset, S. Kubsky, F. Sirotti, *TEMPO: a New Insertion Device Beamline at SOLEIL for Time Resolved Photoelectron Spectroscopy Experiments on Solids and Interfaces*, paper presented at the SRI 2009, 10th International Conference on Synchrotron Radiation Instrumentation, Melbourne, Australia, 27 September - 2 October 2009. 1234: 185-188. (2010).

[17] https://www.diamond.ac.uk/Instruments/Spectroscopy/B18/Station.html

[18] C. Meneghini, L. Leboffe, M. Bionducci, G. Fanali, M. Meli, G. Colombo, M. Fasano, P. Ascenzi, S. Mobilio, *PLOS ONE*, **2015**, *10(3)*, e0123144.

[19] M. Benfatto, C. Meneghini in *A Close Look into the Low Energy Region of the XAS Spectra: The XANES Region* In *Synchrotron Radiation* (Eds.: S. Mobilio, F. Boscherini, C. Meneghini) Springer, Berlin, Heidelberg **2015**.

[20] C. Meneghini, F. Bardelli, S. Mobilio, *Nucl. Instum. Methods Phys. Res. Sect. B Interact. Mater. At.* **2012**, *285*, 153.

[21] G. Bunker, *Introduction to XAFS: A Practical Guide to X-ray Absorption Fine Structure Spectroscopy*, Cambridge: *Cambridge University Press,* **2010**.

[22] D.E. Sayers, E.A. Stern, F.W. Lytle, *Phys. Rev. Lett.* **1971**, *27*, 1204.

[23] A.L. Ankudinov, B. Ravel, J.J. Rehr, S.D. Conradson, *Phys. Rev.* **1998**, *B 58*, 7565.

[24] D.T. Clark D. Kilcast W.K.R. Musgrave, *J. Chem. Soc. Chem. Commun*. **1971**, *517.*

[25] J.C. Klein, C.P. Li, D.M. Hercules, J.F. Black, *Appl. Spectrosc.* **1984**, *38*, 729.

[26] L. Kau, D.J. Spira-Solomon, J.E. Penner-Hahn, K.O. Hodgson, E.L. Solomon, *J. Am. Chem. Soc.*, **1987**, *109*, 6433.

[27] R. Khan, M. Usman, R. Dhivya, P. Balaji, A. Alsame, H. AlLohedan, F. Arjmand, K. AlFarhan, M.A. Akbarsha, F. Marchetti, C. Pettinari, S. Tabassum, *Sci Rep* **2017**, *7*, 45229.

[28] K. Fujisawa, Y. Noguchi, Y. Miyashita, K. Okamoto, N. Lehnert. , *Inorg. Chem.* **2007**, *46*, *25*, 10607.

[29] J.-C. Castillo, N.-F. Bravo, L.-V. Tamayo, P.-D. Mestizo, J. Hurtado, M. Macías, J. Portilla, *ACS Omega* **2020**, *5*, *46*, 30148.

[30] N.J. Blackburn, R.W. Strange, J. Reedijk, A. Volbeda, A. Farooq, K.D. Karlin, J. Zubieta, *Inorg. Chem.* **1989**, *28*, 1349.

[31] J. Rudolph, C.R. Jacob, *Inorg. Chem.* **2018**, *57*, 10591.

[32] J. J. Rehr, R. C. Albers, *Rev. Mod. Phys.* **2000**, *72*, 621.

[33] M. Pellei, C. Santini, L. Bagnarelli, C. Battocchio, G. Iucci, I. Venditti, C. Meneghini, S. Amatori, P. Sgarbossa, C. Marzano, M. De Franco, V. Gandin, *Int. J. Mol. Sci.* **2022**, *23(16)*, 9397.

[34] L. Binelli, V. Dini, S. Amatori, T. Scotognella, A. Giordano, B. De Berardis B., F. Bertelà, C. Battocchio, G. Iucci, I. Fratoddi, A. Cartoni, I. Venditti, Nanomaterials **2023**, *13(13)*, 1898.

[35] R. Mukherjee, in *Comprehensive Coordination Chemistry II* (Eds.: J. A. McCleverty and T. J. Meyer) Pergamon, Oxford, **2003**, pp. 747-910.

[36] I. Schiesaro, I. Venditti, M. Pellei, C. Santini, L. Bagnarelli, G. Iucci, C. Battocchio, C. Meneghini in *Metal Coordination Core in Copper(II)*

Complexes Investigated by XAFS (Eds.: A. Di Cicco, G. Giuli, A. Trapananti) *Springer Proceedings in Physics*, Berlin, Heidelberg, **2021**.

[37] P. Swift, D. Shuttleworth, M.P. Seah in *Practical Surface Analysis by Auger and X-ray Photoelectron Spectroscopy*, (Eds.: D. Briggs and M. P. Seah), J. Wiley & Sons, Chichester, **1983**, chapter 4.

Entry for the Table of Contents

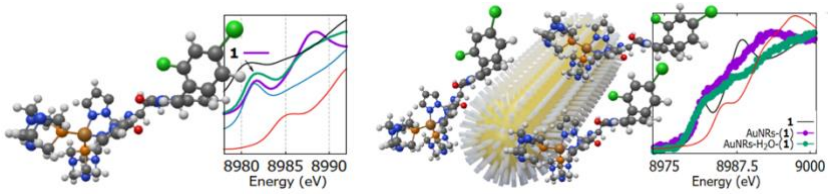

In this work a multi-technique approach based on SR-XPS and XAS allowed to properly define the coordination geometry around the copper ion of Cu(I) coordination compounds, as well as to ascertain the coordination compounds' molecular structures, their stability and, most interesting, the structural modifications arising upon interaction with gold nanoparticles, in both solid and liquid phase.